Hindawi
Journal of Nanomaterials
Volume 2019, Article ID 2458312, 12 pages
https://doi.org/10.1155/2019/2458312

Research Article

Eggshell-Derived Nanohydroxyapatite Adsorbent for Defluoridation of Drinking Water from Bofo of Ethiopia

Kifle Workeneh, Enyew Amare Zereffa, Toshome Abdo Segne, and Rajalakshmanan Eswaramoorthy

Department of Applied Chemistry, School of Applied Natural Science, Adama Science and Technology University, Adama P.O. 1888, Ethiopia

Correspondence should be addressed to Enyew Amare Zereffa; enyewama@yahoo.com and Rajalakshmanan Eswaramoorthy; rajalakshmanan.e@gmail.com

Received 25 March 2019; Revised 3 June 2019; Accepted 1 July 2019; Published 26 August 2019

Guest Editor: Nirupam Aich

Fluoride has become a notable toxicological environmental hazard worldwide because it is often found in groundwater. In the present study, hydroxyapatite adsorbent was synthesized from eggshell waste to remove fluoride from aqueous solution. XRD, FT-IR, and TGA techniques were used to characterize the prepared adsorbent. Batch adsorption studies were performed to examine the adsorption capacity of hydroxyapatite such as the effect of the initial pH of the solution, contact time, adsorbent dose, and initial fluoride concentration. The fluoride ion-selective electrode was used to determine the fluoride removal efficiency. 98.8% of fluoride was removed at pH 3.0, but at pH ~7.0, 85% of fluoride was removed; it shows that the fluoride adsorption is pH dependent. The adsorption isotherm studies (Langmuir and Freundlich models) and the experimental results for the removal of fluoride showed that the Langmuir model was more favorable and the reaction followed pseudo-second-order kinetics. In real water samples, the prepared hydroxyapatite derived from eggshell exhibited 81% removal efficiency. Our results indicate that eggshell waste-derived hydroxyapatite may be an alternative source for defluoridation in developing countries.

1. Introduction

Water is an essential element in human life which may be adulterated by industrial wastes and natural causes. It is estimated that poor quality of drinking water causes 80% of diseases worldwide. It has been reported that 65% of endemic fluorosis is caused by fluoride-contaminated drinking water [1, 2]. Fluoride is vital for mineralization of hard tissues in humans; however, it is harmful when the concentration is higher than 1.5 mg/L. Excess fluoride ions (>1.5 mg/L) are strongly attracted to cationic calcium present in bones and teeth that results in skeletal and dental fluorosis [3, 4]. World Health Organization (WHO) standards suggest that the concentration range of fluoride should be within 1.0 to1.5 ppm in drinking water. However, it has been reported that 11 million individuals living in the Rift Valley region of Ethiopia are highly vulnerable to fluoride-related problems as they rely on drinking water sources having high fluoride concentrations (33 mg/L) [5]. Therefore, developing a cost-effective fluoride removal technique is paramount in developing countries like Ethiopia. Currently, a range of techniques has been used for fluoride removal that includes precipitation, membrane filtration, ion exchange/adsorption, and distillation. However, these fluoride removal techniques have their own drawbacks such as poor removal capacities, lack of selectivity, adverse effects on water quality, production of high volumes of sludge, and complex procedures. Hence, it is critical to develop a cost-effective strategy to remove the surfeit fluoride from the drinking water.

Recently, the adsorption method is shown to be effective in the removal of fluoride even at low concentrations, and additionally, it has low maintenance cost [6–9]. Consequently, a range of low-cost materials has been investigated for their excess fluoride removal efficiency from drinking water. However, all these materials showed poor fluoride adsorption capability and are not enough for wide application. Because

of economic reasons, bone char has been commonly used as adsorbent for defluoridation of drinking water in developing countries [5, 6, 10]. However, challenges on obtaining high-quality bone char materials and hygiene-related issues limited their usage on a large scale worldwide. Recently, several researchers have investigated a range of calcium-based adsorbent materials, of which synthetic hydroxyapatite has been the promising candidate due to its identical chemical composition with bone, nontoxicity, and specifically high fluoride removal capability [11–17]. Recently, researches indicate that HA has better defluoridation capability and the defluoridation efficiency is greatly size dependent on synthetic hydroxyapatite [13, 18, 19]. Traditionally, the preparation of synthetic HA uses any of the following methods such as wet precipitation methods, sol-gel technique, hydrothermal technique, or low-temperature synthesis.

Among them, the wet chemical precipitation method has shown to be advantageous over other methods due to its cost-effective simple procedure [12]. In addition, the main advantage of this method is that it is eco-friendly and water is the only by-product. In general, HA can be synthesized either from biowastes like coral and seashell or from calcium and phosphate source precursors [12, 20, 21]. Eggshells are a naturally occurring calcium source. Daily, a large number of eggshells are left without use and produce waste. More importantly, eggshell supports microbial production that leads to environmental pollution. As per our understanding, only a limited number of researchers have used eggshells for preparing synthetic HA [22–25]. Therefore, in this study, we aimed to synthesize hydroxyapatite from eggshell through wet chemical precipitation and tested for its defluoridation capacity. The removal efficiency of the HA obtained from eggshell was compared with that of commercial HA to assure that eggshell-derived HA powder is a low-cost adsorbent that has the potential to remove excess fluoride from drinking water. In addition, various operating parameters that may influence the adsorption process such as pH, initial concentration of adsorbate, and the amount of adsorbent (HA) used were studied.

2. Materials and Methods

Chicken eggshells were collected from local restaurants in Adama city. Analytical-grade chemicals and reagents were purchased from Addis Ababa (NEWAY PLC, Chemicals). All test solutions were prepared with deionized water.

2.1. Synthesis of Hydroxyapatite. Hydroxyapatite powder was synthesized from eggshell waste and phosphoric acid through wet chemical precipitation in two phases. In phase I, the surface of the eggshells was washed three times with distilled water and the internal thin layer of the shell was removed to decrease the collagens. The cleaned raw shells were boiled in distilled water for 1 hr at 100°C to remove impurities and organic matter. The eggshell was dried in an oven at 80°C for 3 hours in order to crush and grind using a pestle and mortar to obtain a powder. The eggshell residue was sieved with a 150 μm size sieve and calcined in a furnace at 850°C for 2 hr on the ceramic crucible to obtain a fine powder. The prepared powder was analyzed by TGA and XRD to confirm the presence of calcium oxide.

In phase II, a stoichiometric amount of calcined eggshell powder (calcium oxide) and 0.3 M H_3PO_4 (to obtain the Ca/P mole ratio equal to 1.67) was added and dispersed in distilled water in a 500 mL beaker. Analytical-grade phosphoric acid was diluted to 0.3 M and added dropwise into the suspension at room temperature by monitoring the pH with a pH meter until the pH reaches 8.5. The solution was subjected to aging treatment for 12 hr at room temperature followed by stirring on a magnetic stirrer for 30 minutes without heating and left for an extra 10 hr for precipitate formation. The precipitate was washed and filtered using a filter (Whitman # 1) paper. Finally, the precipitate obtained was dried in an oven at 80°C for 3 hr and calcined (900°C) in a furnace on a ceramic crucible for 2 hr to obtain the hydroxyapatite (HA) powder. The synthesized HA powder was stored in a dry place and taken for further characterization.

2.2. Thermogravimetric Analysis (TGA). TGA analysis was used (Shimadzu DTG-60 Plus instrument) for the determination of the calcination temperatures. The prepared eggshell and synthesized HA powders were sieved with a 50 μm size sieve, and 10 mg of each sample was weighed on an electronic mass balance and placed in the alumina crucible for TGA/DTA analysis under an air atmosphere at a heating rate of 10°C/minute.

2.3. XRD Analysis. The HA samples were grounded using a marble mortar and pestle before distributing 100 mg of the ground sample powder over a 10 mm diameter. The prepared HA samples were analyzed by XRD using a CuKα monochromatic beam (wavelength = 0.154056 nm) produced at 40 kV and 30 mA. The XRD spectrum was recorded from 10° to 80° with 2θ angles.

2.4. Phase Identification. For the phase identification step, the X-ray diffraction patterns were directly compared to the files to HA from the Joint Committee Powder Diffraction Standards (JCPDS, card no. 09-432) as was supplied by the International Centre for Diffraction Data (ICDD).

2.5. Crystal Size. Scherrer's formula was used to determine the crystal size from the XRD pattern. As per this equation, a single crystal dimension (nm) can be calculated from the peak broadening.

$$D = \left(\frac{K\alpha}{\text{FWHM}}\right)\theta. \quad (1)$$

In the above equation, D is the crystal size (nm), K is the Scherrer constant (0.9 for hexagonal HA), α is the wavelength of the monochromatic X-ray beam (0.15418 nm), and FWHM is the experimental full width at half maximum intensity of the diffraction peak under the consideration peak; θ is the diffraction angle (°).

2.6. Fourier Transform Infrared (FT-IR) Spectroscopy. Fourier transform infrared spectroscopy (FT-IR) was handled by a Spectrum 65 FT-IR (PerkinElmer). Sample preparation was

done by mixing 2 mg of each sample with 300 mg of potassium bromide (KBr), compressed to form a pellet and then placed on a specimen holder; the spectrum was recorded from 400 to 4000 cm^{-1}.

2.7. Sample Preparation of Synthesized HA for the Defluoridation Test. After characterization of the synthesized HA, four samples of the powder were accurately weighed on an electronic mass balance for the defluoridation test. The samples have constant intervals of 1 g, 3 g, 5 g, and 7 g.

2.8. Preparation of Stock Solution for the Defluoridation Test. Fluoride stock solution was prepared by dissolving 2.21 g of sodium fluoride in 1000 mL of distilled water in a plastic standard flask. Equal intervals of fluoride solutions of 5, 10, 15, and 20 mg/L fluoride were prepared by serial dilution from the stock solution for the defluoridation test.

2.9. Preparation of the Raw Water Sample for the Defluoridation Test. Six samples (30 mL) of groundwater (raw water) were donated from Bofo and Serenity sites under the supervision of OSHO Lab Technical for the practical defluoridation test. Three samples from Bofo located at East Shewa, Lome district, and three samples from Serenity located at East Shew around Meki town were carefully measured with the graduated cylinder and kept in a 50 mL plastic beaker until their fluoride concentration was determined. The fluoride concentrations of water samples were 8.3 and 10.5 mg/L, respectively, and both are above the WHO guideline. The defluoridation test was done with 1, 3, and 5 g doses of synthesized HA powder by using the same procedure for optimizations.

2.10. Preparation of TISAB (Total Ionic Strength Adjustment Buffer). TISAB is essential in ion-selective electrode measurements because it masks minor changes made in the ionic strength of the solution and hence increases the accuracy of the reading. 7 g trisodium citrate ($Na_2C_6H_2O_7$), 56 g sodium chloride (NaCl), and 2 g EDTA are dissolved into 500 mL of double-distilled water. After the solution was dissolved, 57 g of glacial acetic acid is added into it, and finally, 5 M sodium hydroxide was added until the pH reached 5.3, then transferred to a 1000 mL volumetric flask, and brought up to the mark using double-distilled water.

2.11. Calibration of the Electrode. 20 mL of fluoride solution with different fluoride ion concentrations was prepared in constant intervals, and 2 mL of TISAB was added to each solution. The potential (E in mV) versus the logarithm of concentration ($\log c$) in mg/L was plotted. The slope of the graph and R^2 were calculated to check the accuracy of the measurement. The prepared concentrations of 2.5, 5, 7.5, and 10 mg/L of fluoride were used for calibration.

2.12. Fluoride Determination Technique. A fluoride ion-selective electrode was used to determine the fluoride ion concentration. For this test, the HA powders were separately added on to 30 mL of the known concentration of fluoride water (5, 10, 15, and 20 mg/L) in a 50 mL plastic beaker. To eliminate the interference effect of complex ions in the solution and to maintain ionic strength and the pH, 2 mL of total ionic strength adjustment buffer (TISAB) solution (10 : 1 volumetric ratio) was added. In this way, the effect of various parameters like contact time, pH, adsorbent dose, and initial fluoride concentration was obtained by changing a parameter and keeping the other parameters constant. Finally, the equilibrium fluoride concentration (residual) for each test was determined using a pH meter in combination with a fluoride-selective electrode, and the pH was measured with a pH meter. The electrode was calibrated prior to each experiment.

2.13. Defluoridation Test. All experiments were conducted using 30 mL of fluoride solution (10 mg/L) taken in four different 50 mL plastic beakers. 1 g, 3 g, 5 g, and 7 g HA samples were added in this solution for different contact times. Then, the solution was stirred for 1 minute at 25°C to reach equilibrium on a homogenous solution. Each sample was taken at a specified time interval for their contact times 1 hr, 3 hr, 5 hr, 7 hr, 11 hr, and 24 hr and filtered with a Whitman filter paper (no. 1) before analysis. The fluoride-selective electrode reads the electrovolt in terms of a millivolt. The millivolt was converted into mg/L of residual fluoride concentration using predetermined calibration slop by Microsoft Excel. The percentage of adsorption efficiency and the fluoride removal capacity (mg of fluoride ion adsorbed per gram of adsorbent) at a given contact time for the HA adsorbent was calculated using the following:

$$\begin{aligned} \text{Percentage removal} &= \frac{[C_o - C_t]}{C_o} \times 100, \\ \text{Adsorption capacity} &= \frac{[C_o - C_t]}{m} \times V. \end{aligned} \tag{2}$$

In the above equation, C_o and C_t are the initial and final fluoride concentrations, respectively, m is the mass of the adsorbent HA, and V is the volume of the solution.

2.14. Optimization of Different Parameters. In this study, the effect of major parameters like adsorbent dose, initial fluoride concentration, contact time, and pH was optimized to investigate the maximum defluoridation efficiency of the synthesized natural hydroxyapatite (HA) from the eggshell.

2.14.1. Effect of Adsorbent Dosage. Experimental examinations were carried at different concentrations of 1, 3, 5, and 7 g of adsorbent in 10 mg/L of fluoride initial concentration at pH 3.

2.14.2. Effect of Contact Time. Residual anionic fluoride concentration was measured at different contact times of adsorption, 1, 3, 5, 7, 11, and 24 hours, with 5 g of adsorbent (HA) to study the effect of contact time. Other parameters like pH, the concentration of the solution, and HA dosage remain constant.

2.14.3. Effect of Initial Fluoride Concentration. To study the effect of initial fluoride concentration, experiments were conducted at various fluoride concentrations (5, 10, 15, and

Table 1: Dimensionless separation factors (R_L).

Concentration (mg/L)	5	10	15	20
R_L	0.235	0.136	0.095	0.073

20 mg/L) at a constant temperature, pH (pH 3), adsorbent dose (5 g), and contact time (5 hr).

2.14.4. Effect of pH. To investigate the effect of pH on defluoridation, the test solutions containing the optimized concentration of fluoride were changed to pH values of 3, 5, 7, and 9 using HCl (1 N) and NaOH (1 N) and the adsorbent mass remained constant through acidic, neutral, and basic media. Then, the determined 5 g HA was added in into each test solution separately and stirred for 1 minute to reach equilibrium. Residual F^- ion concentrations were evaluated in each experiment after 5 hr contact time. Finally, pH versus percentage removal graph was plotted to explain the adsorption performance of the adsorbent HA at each pH.

2.15. Adsorption Isotherm Models. The relationship between the amounts of substances sorbed at a constant temperature and its concentration equilibrium solution is called adsorption isotherm. The frequently used adsorption isotherm models for surface average analysis are Langmuir and Freundlich isotherms.

2.15.1. Langmuir Adsorption Isotherm. The Langmuir isotherm model is widely used to quantify the amount adsorbed on the adsorbent as a function of concentration at a given temperature. Theoretically, the adsorbent has a limited number of available sites for the adsorbate. Therefore, beyond saturation value, no further adsorption can occur. The linear form of the Langmuir is as follows:

$$\frac{C_e}{q_e} = \frac{C_e}{q_e} + \frac{1}{b}. \quad (3)$$

The Langmuir isotherm can be expressed by a dimensionless separation factor or equilibrium parameter, R_L, which is defined by

$$R_L = \frac{1}{1 + C_{ob}}. \quad (4)$$

The value of R_L indicates the type of isotherm which is either favorable ($0 < R_L < 1$), unfavorable ($R_L > 1$), or irreversible ($R_L = 0$) (Tables 1 and 2).

2.15.2. Freundlich Adsorption Isotherm. The Freundlich isotherm equation takes into account repulsive interactions between adsorbed solute particles and also accounts for surface heterogeneities. The logarithm form of the Freundlich isotherm is given as follows:

$$\text{Log}q_e = \frac{1}{n} \log C_e + \log \text{kf}. \quad (5)$$

Table 2: Kinetic data obtained by varying the contact time using a constant adsorbent dose of 5 g HA, pH = 3, and 10 mg/g of fluoride concentration.

Time (hr)	Residual fluoride	q_t (mg/g)	t/q_t	$\ln(q_e - q_t)$	$\ln q_t$
1	0.15	0.0591	16.92047	-8.1117	-2.82855
3	0.12	0.0592	58.67567	-8.5171	-2.8265
5	0.10	0.0594	84.17508	∞	-2.8234
7	0.11	0.0593	118.04384	-9.2103	-2.8251
9	0.11	0.0592	151.77065	-9.2103	-1.8251
11	0.13	0.0592	185.81081	-8.5171	-2.8268
24	0.13	0.0592	405.40545	-8.5171	-2.8268

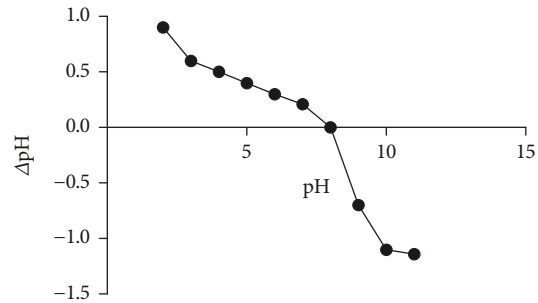

Figure 1: Plot of ΔpH vs. final pH of the adsorbent to determine the point of zero charges.

Finally, the applicability of two adsorption isotherms (Langmuir and Freundlich) can be compared by evaluating the multiple regression correlation coefficients, R^2 (Table 2).

2.16. pH at the Potential of Point of Zero Charges (pH_{pzc}) Determination. The isoelectric point or point of zero charges (pH_{pzc}) were determined by using the reported method [26]. Ten NaCl (0.1 M) solutions with an initial pH range of 2–11 were prepared in duplicate. Each duplicate was added with 2 g of HA and mixed for 0.5 hr. Then, the adsorbent was separated from the solutions by filtration. The final pH values of the 10 solutions were measured by a pH meter and therefore calculation of ΔpH (ΔpH = final pH − initial pH). A graph of final pH values plotted against ΔpH is shown in Figure 1. The pH_{pzc} (point of zero charges) of the adsorbent was determined from the plotted graph (Table 3).

2.17. Kinetics of Adsorption. It is very important to know the rate at which the adsorption process takes place and the factors that control the rate of the process; for this purpose, the kinetics of the process were evaluated. The adsorption kinetic studies describe the rate of uptake of the adsorbate molecule; in this case, fluoride ion onto adsorbent, the rate depends on the physicochemical characteristics of the adsorbate and adsorbent, pH, temperature, and concentration. To describe the adsorption kinetic behavior, the following models are used.

Table 3: ΔpH vs. final pH of the adsorbent perfumed on 2 g HA, 10 mg/L of fluoride concentration, and 5 hr contact time.

Initial pH	2	3	4	5	6	7	8	9	10	11
Final pH	2.90	3.60	4.50	5.40	6.30	7.21	7.90	8.30	8.90	9.86
Change in pH	0.90	0.60	0.50	0.40	0.30	0.21	0	-0.7	-1.1	-1.14

Table 4: Adsorption kinetic parameter for pseudo-first-order kinetics.

Pseudo-first-order kinetics	Intercept	K_1	R^2	q_e
	-8.634	0.005	0.0089	-0.1602

Table 5: Adsorption kinetic parameter for pseudo-second-order kinetics.

Pseudo-second-order kinetics	Intercept	K_2	R^2	q_e
	2.1152	134.048	0.999	0.0596

2.17.1. Pseudo-First-Order Equation. The pseudo-first-order differential equation is generally expressed as follows [27]:

$$\frac{dq}{dt} = K_1 (q_e - q_t). \tag{6}$$

In the above equation, q_e and q_t refer to the amount of fluoride ion adsorbed per unit mass of the adsorbate at equilibrium time and any time (mg/g), respectively. K_1 is the rate constant of pseudo-first-order adsorption. Integrating equation (6) by applying the boundary conditions $q_e = 0$ at $t = 0$ and $q_t = q$ to obtain the following linear equation t at $t = t$ gives

$$\frac{\text{Log}q_e}{q_e - q_t} = \frac{K_1 t}{2.303}. \tag{7}$$

Equation (7) can be rearranged and described by ln.

$$\ln (q_e - q_t) = \ln q_e - K_1 t. \tag{8}$$

The rate constant K_1 and equilibrium adsorption capacity q_e can be predicted from the slope and intercept, respectively, of the linear plots of $\log (q_e - q_t)$ versus t (Table 4).

2.17.2. Pseudo-Second-Order Equation. The rate of a pseudo-second-order differential equation is given as follows [28, 29]:

$$\frac{dq_t}{dt} K_2 (q_e - q_t)^2, \tag{9}$$

where K_2 is the rate constant of the pseudo-second-order equation (g/mg·min.) and q_e is the equilibrium adsorption capacity (mg/g). By applying the boundary conditions $q_t = 0$ at $t = 0$ and $q_t = q_t$ at $t = t$ on equation (9) and rearranging, the following linearized equation is obtained:

$$\frac{t}{q_t} = \frac{t}{q_t} + \frac{1}{K^2 {q_e}^2}. \tag{10}$$

The values of q_t and K^2 can be determined experimentally from the slope and intercept, respectively, of the plots of t/q_t versus t (Table 5).

3. Results and Discussion

3.1. Characterization of the Calcium Precursor Material (Eggshell Powder). The calcium precursor used for the HA synthesis was derived from the decomposition of eggshell. The complete calcium precursor decomposition temperature was obtained from the TGA/DTA result. The thermogravimetric analysis (TGA) of the eggshell powder was carried out between room temperature and 1000°C in order to determine the thermal stability and the decomposition temperature of eggshell powder. The TGA result revealed that a significant mass loss was observed between the temperatures 600 and 800°C, probably due to the removal of impurities, and the eggshell residue was stable above 800°C as indicated in Figure 2. XRD diffraction graph of calcined eggshell residue at 850°C is shown in Figure 3. The diffraction peaks at 34.078°, 37.123°, 54.351°, and 63.613° corresponding to (111), (200), (220), and (311) planes, respectively, shown on the graph are in good agreement with the reported standard values of CaO [30].

3.2. Characterization of HA Powder. TGA/DTA experiments were done to determine the calcination temperature for the formation of pure-phase hydroxyapatite synthesized from calcined eggshell residue and phosphoric acid. As illustrated in Figure 4, the result revealed that the material is stable or has no significant mass loss above 900°C. The XRD pattern of HA powder obtained after calcination at 900°C is shown in Figure 5. According to the figure, there is no peak attributable to possible impurities, which indicates that the final product is highly pure HA according to the ICDD powder diffraction file (pdf number 009-0432). All possible peaks can be indexed to the pure hexagonal phase of HA (P63mc) without secondary phases such as α-TCP (alpha-tricalcium phosphate) and β-TCP (beta-tricalcium phosphate). This confirmed the successful synthesis of pure-phase HA via the chemical precipitation from calcined eggshell residue. The crystallite size was calculated using Scherer's formula from the XRD pattern. The calculated single crystallite sizes were D1 = 50.5, D2 = 45.2, and D3 = 48.7 nm, and the average crystal size obtained was 48.13 nm. The FT-IR spectrum shows band 3444 cm^{-1} of the OH^- bond stretching (Figure 6). The intensified peak in the region between 1414 and 1040 cm^{-1} is attributed to the phosphate group. The

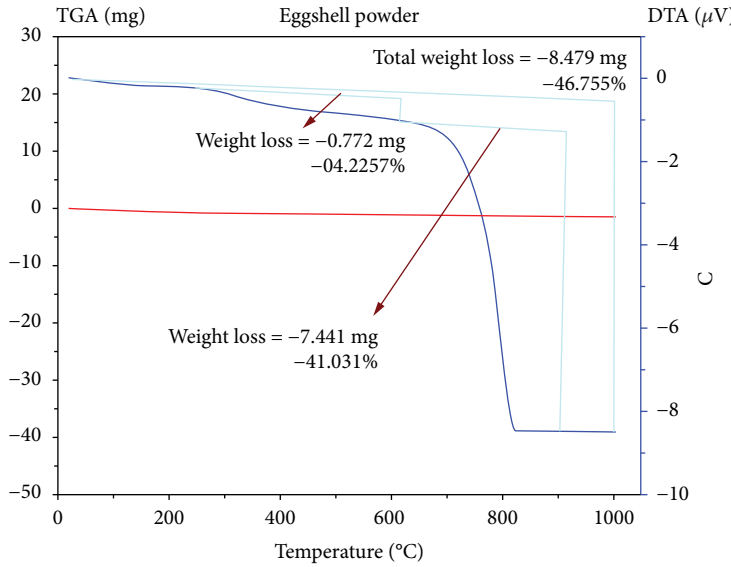

Figure 2: TGA/DTA result of eggshell powder.

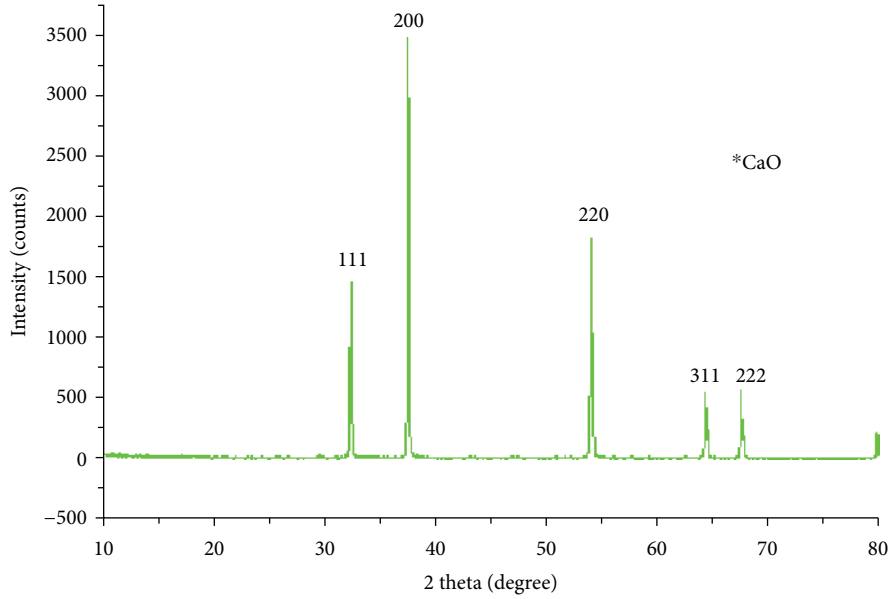

Figure 3: XRD pattern of calcinated eggshell at 850°C.

band at 595 cm^{-1} belongs to the phosphate group. These peaks confirm that the phosphate group occupies two sites in the crystal lattice [11, 31].

3.3. Defluoridation Efficacy of HA on Prepared Fluoride Solution

3.3.1. Determination of the Adsorbent Dose (HA). The concentration range was selected based on the preliminary test results at room temperature. The experiment was conducted on different masses of adsorbent at 1 g 3 g, 5 g, and 7 g in 10 mg/L of the initial fluoride concentration with 5 hr contact time at pH 3. As described in Figure 7, the fluoride removal efficiency is directly proportional to the adsorbent dose up to 5 g because of a large number of fluoride-binding site availability. As identified, the equilibrium was fully established at a 5 g dose with high fluoride removal of about 99%. When the initial fluoride concentration is 10 mg, the equilibrium fluoride concentration falls within the WHO limit and there is no significant change on the efficiency beyond this 5 g adsorbent dose. Therefore, for further adsorption experimentation, 5 g of HA was considered as an ideal dose. The adsorption versus percentage removal of fluoride is given in Figure 7. The experimental result of different HA doses exhibited increases with adsorbent dosage, until it is equal to 5 g, then decreases, when the dosage is increased to 7 g. The results

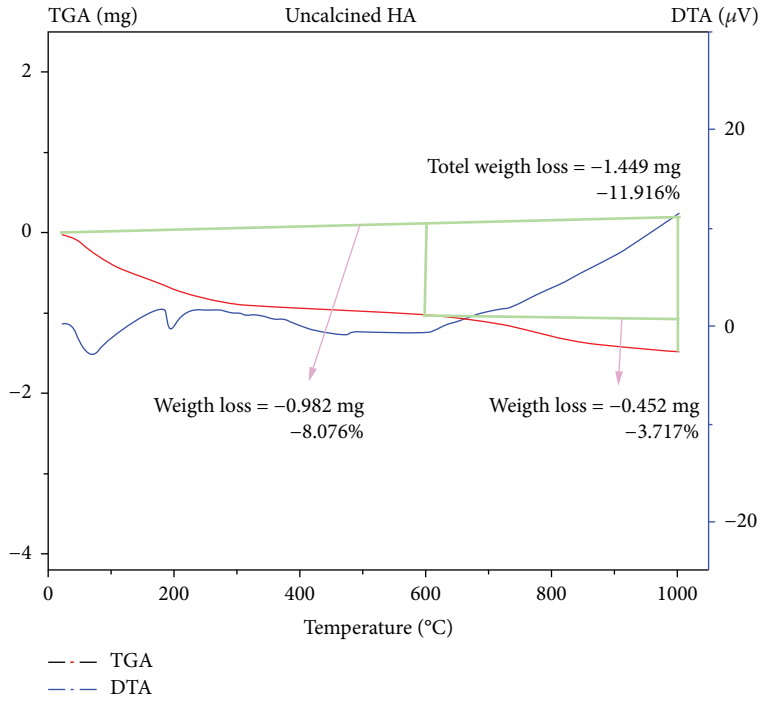

Figure 4: TGA/DTA pattern for the synthesized HA.

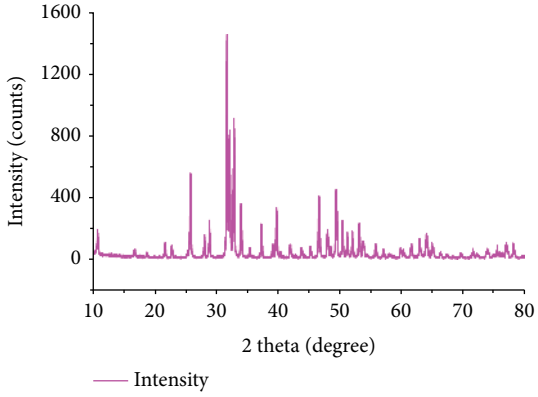

Figure 5: XRD pattern of HA powder calcined at 900°C.

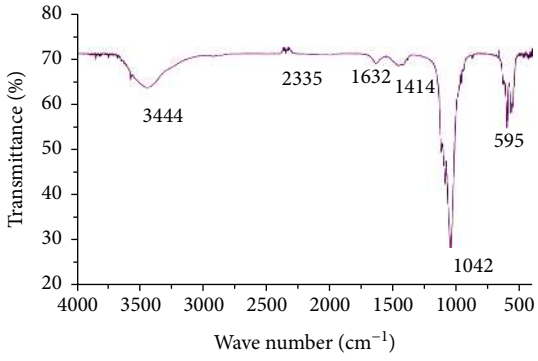

Figure 6: FT-IR patterns of calcinated HA powder.

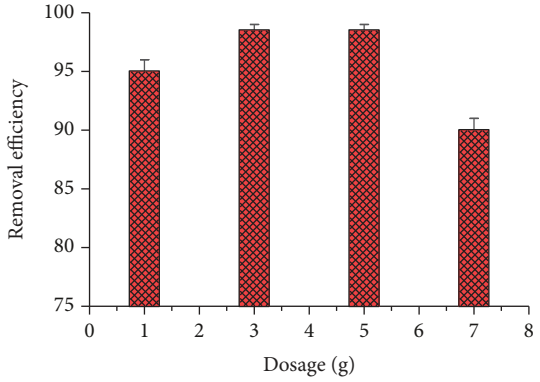

Figure 7: Investigation of the optimum dose test using 10 mg/L initial fluoride concentration, pH 3, and contact time of 5 hr.

show that an increase in adsorbent dosage results in increasing of fluoride removal efficiency because of the increased availability of fluoride-binding sites. The decrease in removal at a 7 g dose is due to the depletion of fluoride in the solution with an increasing dose of the adsorbent.

3.3.2. Determination of Contact Time. To determine the effect of contact time on adsorption of fluoride on hydroxyapatite, batch experiments were carried with different contact times (1 hr, 3 hr, 5 hr, 7 hr, 9 hr, and 11 hr) under constant dosage (5 g, 10 g/L fluoride concentration) and pH (pH 3) at room temperature. As shown in Figure 8, rapid fluoride removal was observed at the initial stage until reaching equilibrium time (5 hours) with a high removal efficiency of about 99%.

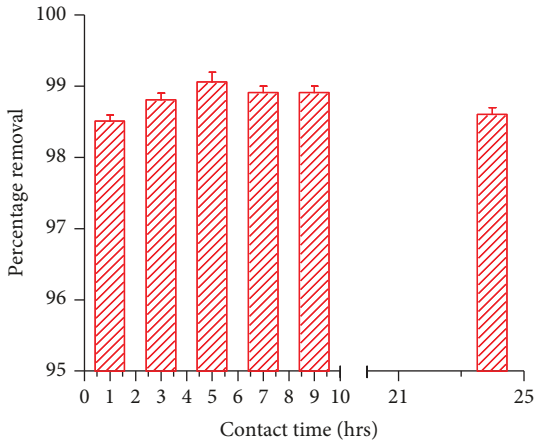

Figure 8: Fluoride removal efficiency as a function of contact time at 5 g of the HA dose, pH = 3, and initial concentration of 10 mg/L.

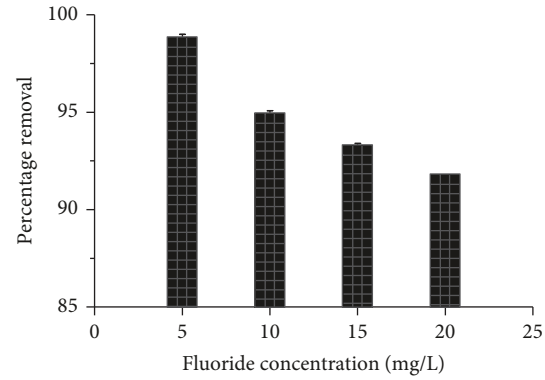

Figure 9: The effect of initial fluoride concentration on percentage removal of fluoride using 5 g adsorbent, 5 hr contact time, and pH = 3.

This is because a high number of active sites at the initial stage lead to high diffusion of fluoride towards the adsorbent surface, as shown in the figure after the equilibrium time slowly desorbed from the surface of the adsorbent to the solution. Therefore, this parameter determines the rate of mass transfer from the solution to the surface of the adsorbent, and the data were used to study the kinetic study of batch adsorption. This trend was also reported by other studies on defluoridation processes [11, 18]. This is due to the faster saturation of the active sites with time. This implies that the adsorbent has a specific number of active sites, which eventually are saturated after prolonged exposure to fluoride solution. After saturation of the active sites, no further adsorption is carried out on the residual fluoride concentration (Figure 8).

3.3.3. Determination of Initial Fluoride Concentration. For this test, the initial concentration of fluoride is selected randomly with 5 increments from 5 to 20 mg/L. The effects of other parameters remain constant, and the adsorbent dose was 5 g with 30 mL solution. The results indicate that the initial fluoride concentration has an influence on the removal capacity of the adsorbent (Figure 9). For a given mass of HA, the fluoride removal capacity decreases with increasing initial concentration because of the increased diffusion of fluoride to adsorption sites and utilization of less active sites of the adsorbent. The optimized result is selected as 10 mg/L which encountered 95% removal efficiency, and the residual fluoride concentration was 0.5 which satisfied the optimum WHO guideline for drinking water.

3.3.4. The Effect of pH on Percentage Removal of Fluoride. The adsorption process is controlled by the pH of the adsorbate solution. To make inclusive all the 3 media, the pH range was deliberately selected from 3 to 9. The effect of pH was investigated by varying the pH from 3 to 9 with 2 increments. As illustrated in Figure 10(a), the maximum defluoridation was achieved at pH 3 which is 98.8%. A decrease in the fluoride removal extent of the adsorbent was observed at increasing pH. The main reason behind the maximum defluoridation at low pH values may be because of the presence of a large number of H^+ ions at these pH values. This leads to neutralization of the OH^- ions on the adsorbed surface and hence reduction of the hindrance to the diffusion of fluoride ions. Therefore, pH is determinant to drinking water, and hence, the optimum removal efficiency for this adsorbent HA was 85% observed on pH = 7.

3.4. Synthesized HA on Raw Water Defluoridation. Samples of water were collected from two different locations of the Oromia region, East Showa district, near Adama city. Sample 1 is from Bofo around the Bati Lome District and sample 2 from around Maki Town; the secured groundwater had fluoride ion concentration of 8.3 mg/L and 10.5 mg/L, respectively, which is still more than the permissible limit of WHO. After adsorption, the fluoride ion concentration of the two samples was measured and it was found that the fluoride ion concentration was decreased significantly in adsorbent doses of 1 g, 3 g, and 5 g, at a temperature of 25°C, rotation speed of 400 rpm for 1 minute steering time, 5 h contact time, and optimum pH = 7 adjusted by a drop of 1 M NaOH. The HA adsorbent almost had good removal efficiency for field samples on the comparable condition to the result obtained on the fluoride solution test. In this paper, it was observed that on the two sites, the synthesized HA material shows fluoride removal efficiencies of 81.92 and 82. 85% for Bofo and Maki, respectively, upon addition of a 5 g dose and at pH 7. The synthesized HA from eggshell waste shows comparable fluoride removal efficiency values to the commercial HA (Figure 10(b)). The final pH of the treated water was found in the range of 7.5 to 8.

3.5. Experimental Result on Adsorption Isotherm. In this investigation, the data based on the optimized fluoride concentration were interpreted in Table 6. As can be observed from the table, $R^2 = 0.97$ is less than one, and hence, the adsorption favors the Langmuir adsorption isotherm model. To determine whether the adsorption favors the Langmuir or the Freundlich model, we can apply the comparison ofR^2 or R_L favoring Langmuir's $(0 < R_L < 1)$, unfavorable $(R_L > 1)$, or irreversible $(R_L = 0)$ [32, 33]. Therefore, as we can observe

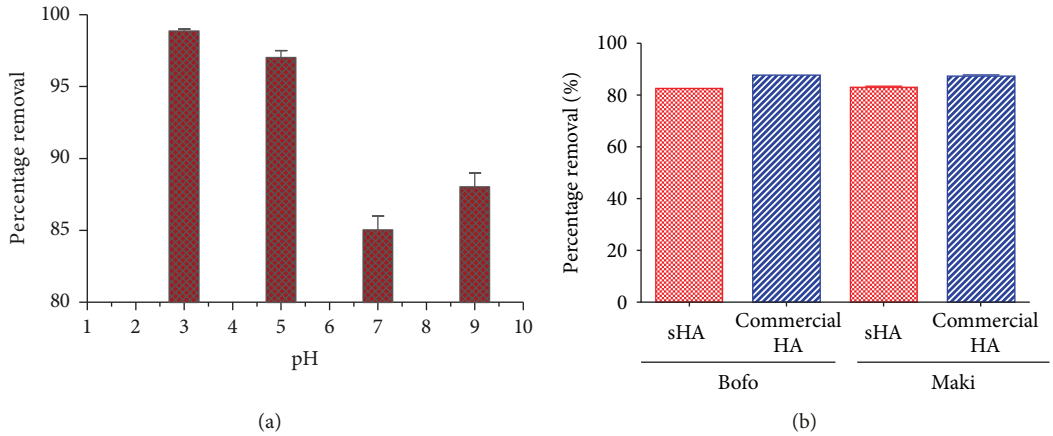

Figure 10: (a) The effect of pH on the percentage removal of fluoride at 5 g adsorbent and 5 hr. (b) Fluoride removal efficiency of synthesized HA (sHA) and commercial HA on raw water samples from Bofo and Maki (5 g dose, 5 hr contact time, and pH 7).

Table 6: Langmuir's adsorption isotherm data for concentration versus adsorption capacity.

C_o (mg/L)	C_e	q_e	log C_e	log q_e	C_e/q_e
5	0.25	0.0285	-0.6020	-1.5451	8.7719
10	0.50	0.0570	-0.3010	-1.2441	8.7719
15	0.96	0.0842	-0.0177	-1.0746	11.4014
20	1.6	0.1104	-0.2041	-0.9570	14.4927

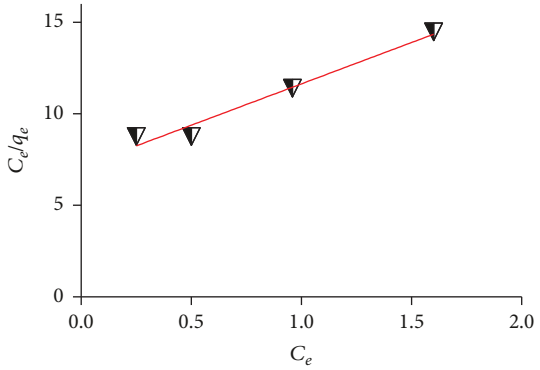

Figure 11: Linearized Langmuir adsorption isotherm for fluoride adsorption.

from the R^2 value, which is 0.96 which is less than one, the adsorption isothermal obeys Langmuir's model (Figure 11). The value of correlation coefficients ($R^2 = 0.9657$) for the Langmuir isotherm is higher in comparison to that obtained for the Freundlich isotherm. For the Freundlich model, the value of correlation coefficient (R^2) was 0.763 (Figure 12). The maximum adsorption capacity of the adsorbent for the Langmuir isotherm is greater than that for the Freundlich model (Tables 1 and 7). Hence, it can be concluded that the Langmuir isotherm model is more suitable for adsorption of fluoride ions than the Freundlich isotherm on the basis of the experimental study.

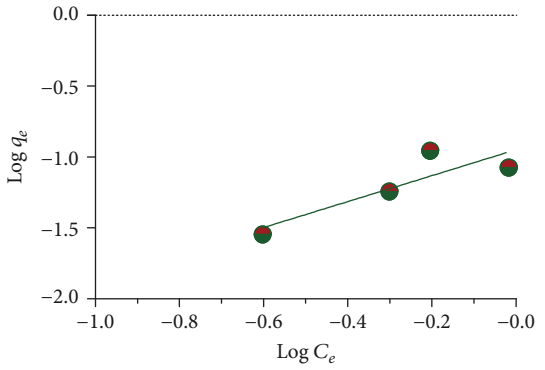

Figure 12: Freundlich isotherm graph of adsorption fluoride by HA.

Table 7: Langmuir and Freundlich isotherm model parameters describing the HA fluoride adsorption at a constant adsorbent dose of 5 g, contact time of 5 hr, and pH = 3.

Parameter	Langmuir model	Parameter	Freundlich model
q (mg/g)	0.2212	kf	0.3879
b (L/mg)	0.6349	$1/n$	0.914
R^2	0.9657	R^2	0.763

3.6. Adsorption Kinetic Models. In the present study, the kinetics of defluoridation was carried out to study the behavior of the synthesized hydroxyapatite Table 2.

3.6.1. Pseudo First-Order Kinetic Model. The different parameters of pseudo-first- and pseudo-second-order kinetics are given in Tables 4 and 5, respectively.

$$\log (q_e - q_t) = \log q_e - \frac{K_1}{2.303} t. \quad (11)$$

For kinetic studies, 5 g of HA would be contacted with 30 mL of fluoride solution having a fluoride concentration

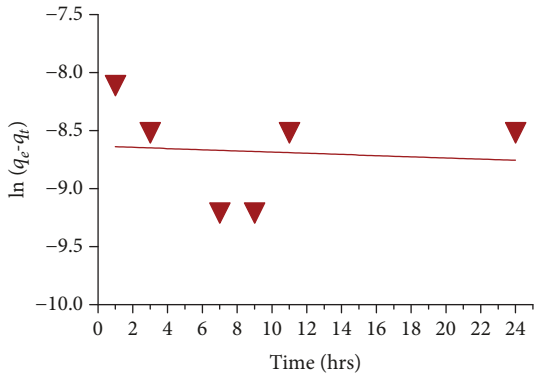

Figure 13: Pseudo-first-order kinetic result.

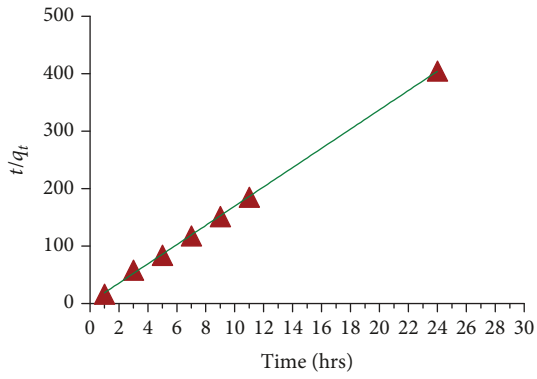

Figure 14: Pseudo-second-order kinetic result.

of 10 g, at a pH of 3, and shaken at 200 rpm and room temperature (Table 4). In the true first order, log q_e should be equal to the intercept as it can be observed from the graphs (Figure 13). Lower correlation coefficients are obtained indicating that the adsorption of fluoride ion on the adsorbent hydroxyapatite does not follow the pseudo-first-order kinetics.

3.6.2. Pseudo-Second-Order Kinetic Model. From the result of adsorption kinetic first-order and second-order data, it is possible to summarize the adsorption behavior of the adsorbents prepared (Table 5). The correlation coefficient (R^2) was found to be 0.0089 and 0.999 for pseudo-first-order kinetics and pseudo-second-order kinetics, respectively. The value of R^2 for pseudo-second-order kinetics approaches to one (Figure 14). The experimental equilibrium adsorption capacity and the calculated capacity are close to the R^2 value of 0.999 [34]. This indicated that it is unity and the adequate linear fitting of the plots confirmed that the adsorption of fluoride ions using the synthesized hydroxyapatite followed pseudo-second-order kinetics [15, 18].

3.7. pH at the Potential of Point of Zero Charge (pH_{pzc}) Determinations. pH_{pzc} is the pH value at the point where the net surface charge of the adsorbent is 0. pH_{pzc} values for the synthesized HA powder at an optimized operational parameter are around 7.90 (Table 3). In general, the pH values of the adsorbents fall in the acidic to the slightly neutral region. The net surface charge of the adsorbents under pH_{pzc} is positive, while it is negative when above pH_{pzc} (Figure 1). Therefore, determination of the pH_{pzc} value helps to identify the working pH value for adsorption studies. Hence, the adsorbent percent removal capacity increases below the pH_{pzc} value [29, 35].

4. Conclusion

In the present investigation, pure-phase hydroxyapatite was successfully synthesized from chicken eggshell through the wet precipitation method for defluoridation of water by adsorption. The main advantage of this eco-friendly method is that water is the only by-product. The XRD result revealed that the synthesized HA powder was pure phase with a hexagonal structure. The prepared HA (adsorbent) was applied to the real water samples under ideal conditions and found to be effective with 81% fluoride removal efficiency. Our results show that eggshell waste-derived hydroxyapatite may be an alternative source for defluoridation in developing countries. Additionally, natural raw water contains ions that compact with fluoride for adsorption such as HCO_3^-, $SO4^{2-}$, and Cl^-. The effect of these coions should be investigated so that it helps to selectively use the adsorbent in preference to other ions.

Data Availability

The data used to support the findings of this study are available from the corresponding authors upon request.

Conflicts of Interest

The authors declare that they have no conflicts of interest.

Authors' Contributions

The study and the first draft writing were conducted by Kifle Workeneh, and the supervision and edition were done by Prof. Rajalakshmanan Eswaramoorthy. The coauthors Enyew Amare Zereffa and Toshome Abdo Segne participated in analyzing the results and drafting the manuscript.

Acknowledgments

The authors are grateful to the management of Adama Science and Technology University for providing the financial support towards this research work.

References

[1] H. J. Mosha, "Endemic dental fluorosis and the possibilities of defluoridation and fluoridation of water supplies in Tanzania," *Odonto-Stomatologie Tropicale*, vol. 7, no. 2, pp. 89–96, 1984.

[2] S. V. Walvekar and B. A. Qureshi, "Endemic fluorosis and partial defluoridation of water supplies - a public health concern in Kenya," *Community Dentistry and Oral Epidemiology*, vol. 10, no. 3, pp. 156–160, 1982.

[3] M. M. Emamjomeh and M. Sivakumar, "An empirical model for defluoridation by batch monopolar electrocoagulation/-flotation (ECF) process," *Journal of Hazardous Materials*, vol. 131, no. 1-3, pp. 118–125, 2006.

[4] E. Y. Wong and M. K. Stenstrom, "Onsite defluoridation system for drinking water treatment using calcium carbonate," *Journal of Environmental Management*, vol. 216, pp. 270–274, 2018.

[5] A. W. Wagutu, R. Machunda, and Y. A. C. Jande, "Crustacean derived calcium phosphate systems: application in defluoridation of drinking water in East African Rift Valley," *Journal of Hazardous Materials*, vol. 347, pp. 95–105, 2018.

[6] S. Chatterjee, S. Jha, and S. De, "Novel carbonized bone meal for defluoridation of groundwater: batch and column study," *Journal of Environmental Science and Health, Part A: Toxic/Hazardous Substances and Environmental Engineering*, vol. 53, no. 9, pp. 832–846, 2018.

[7] K. S. Hashim, A. Shaw, R. Al Khaddar, M. Ortoneda Pedrola, and D. Phipps, "Defluoridation of drinking water using a new flow column-electrocoagulation reactor (FCER) - experimental, statistical, and economic approach," *Journal of Environmental Management*, vol. 197, pp. 80–88, 2017.

[8] P. Loganathan, S. Vigneswaran, J. Kandasamy, and R. Naidu, "Defluoridation of drinking water using adsorption processes," *Journal of Hazardous Materials*, vol. 248-249, pp. 1–19, 2013.

[9] V. K. Gupta, I. Ali, and V. K. Saini, "Defluoridation of wastewaters using waste carbon slurry," *Water Research*, vol. 41, no. 15, pp. 3307–3316, 2007.

[10] H. Herath, T. Kawakami, and M. Tafu, "The extremely high adsorption capacity of fluoride by chicken bone char (CBC) in defluoridation of drinking water in relation to its finer particle size for better human health," *Healthcare*, vol. 6, no. 4, p. 123, 2018.

[11] Y. Xia, X. Huang, W. Li, Y. Zhang, and Z. Li, "Facile defluoridation of drinking water by forming shell@fluorapatite nanoarray during boiling egg shell," *Journal of Hazardous Materials*, vol. 361, pp. 321–328, 2019.

[12] D. Mehta, P. Mondal, V. K. Saharan, and S. George, "Synthesis of hydroxyapatite nanorods for application in water defluoridation and optimization of process variables: advantage of ultrasonication with precipitation method over conventional method," *Ultrasonics Sonochemistry*, vol. 37, pp. 56–70, 2017.

[13] C. M. Kanno, R. L. Sanders, S. M. Flynn, G. Lessard, and S. C. B. Myneni, "Novel apatite-based sorbent for defluoridation: synthesis and sorption characteristics of nano-microcrystalline hydroxyapatite-coated-limestone," *Environmental Science & Technology*, vol. 48, no. 10, pp. 5798–5807, 2014.

[14] L. Feng, W. Xu, T. Liu, and J. Liu, "Heat regeneration of hydroxyapatite/attapulgite composite beads for defluoridation of drinking water," *Journal of Hazardous Materials*, vol. 221-222, pp. 228–235, 2012.

[15] C. S. Sundaram, N. Viswanathan, and S. Meenakshi, "Defluoridation chemistry of synthetic hydroxyapatite at nano scale: equilibrium and kinetic studies," *Journal of Hazardous Materials*, vol. 155, no. 1-2, pp. 206–215, 2008.

[16] M. J. Larsen and E. I. F. Pearce, "Defluoridation of drinking water by boiling with brushite and calcite," *Caries Research*, vol. 36, no. 5, pp. 341–346, 2002.

[17] B. Ying, X. Li, and Z. Cong, *Wei Sheng Yan Jiu*, vol. 30, no. 6, pp. 326–328, 2001, Study on the defluoridation of drinking water with synthetic hydroxyapatite.

[18] Q. Tang, T. Duan, P. Li, P. Zhang, and D. Wu, "Enhanced defluoridation capacity from aqueous media via hydroxyapatite decorated with carbon nanotube," *Frontiers in Chemistry*, vol. 6, p. 104, 2018.

[19] K. Pandi and N. Viswanathan, "Enhanced defluoridation and facile separation of magnetic nano-hydroxyapatite/alginate composite," *International Journal of Biological Macromolecules*, vol. 80, pp. 341–349, 2015.

[20] X. Li, D. Zheng, and B. Ying, "Manufacture of hydroxyapatite as a defluoridator and the mechanism of defluoridation for drinking water," *Wei Sheng Yan Jiu*, vol. 31, no. 2, pp. 136–138, 2002.

[21] B. Ying, X. Li, D. Zheng, and J. Gao, "Optimizing the synthesis of hydroxyapatite as a method for the defluoridation of drinking water," *Wei Sheng Yan Jiu*, vol. 30, no. 4, pp. 244–246, 2001.

[22] A. C. Ferro and M. Guedes, "Mechanochemical synthesis of hydroxyapatite using cuttlefish bone and chicken eggshell as calcium precursors," *Materials Science & Engineering, C: Materials for Biological Applications*, vol. 97, pp. 124–140, 2019.

[23] V. H. Ingole, K. Hany Hussein, A. A. Kashale et al., "Ultrasound-assisted green economic synthesis of hydroxyapatite nanoparticles using eggshell biowaste and study of mechanical and biological properties for orthopedic applications," *Journal of Biomedical Materials Research Part A*, vol. 105, no. 11, pp. 2935–2947, 2017.

[24] S. K. Padmanabhan, L. Salvatore, F. Gervaso et al., "Synthesis and characterization of collagen scaffolds reinforced by eggshell derived hydroxyapatite for tissue engineering," *Journal of Nanoscience and Nanotechnology*, vol. 15, no. 1, pp. 504–509, 2015.

[25] D. Siva Rama Krishna, A. Siddharthan, S. K. Seshadri, and T. S. Sampath Kumar, "A novel route for synthesis of nanocrystalline hydroxyapatite from eggshell waste," *Journal of Materials Science: Materials in Medicine*, vol. 18, no. 9, pp. 1735–1743, 2007.

[26] S. Alemu, E. Mulugeta, F. Zewge, and B. S. Chandravanshi, "Water defluoridation by aluminium oxide-manganese oxide composite material," *Environmental Technology*, vol. 35, no. 15, pp. 1893–1903, 2014.

[27] S. Muthu Prabhu and S. Meenakshi, "Defluoridation of water using dicarboxylic acids mediated chitosan-polyaniline/-zirconium biopolymeric complex," *International Journal of Biological Macromolecules*, vol. 85, pp. 16–22, 2016.

[28] V. Dhongde, K. L. Wasewar, and B. S. De, "Development of nanohybrid adsorbent for defluoridation from aqueous systems," *Chemosphere*, vol. 188, pp. 354–366, 2017.

[29] K. Parashar, N. Ballav, S. Debnath, K. Pillay, and A. Maity, "Hydrous ZrO_2 decorated polyaniline nanofibres: synthesis, characterization and application as an efficient adsorbent for water defluoridation," *Journal of Colloid and Interface Science*, vol. 508, pp. 342–358, 2017.

[30] L. M. Correia, R. M. A. Saboya, N. de Sousa Campelo et al., "Characterization of calcium oxide catalysts from natural sources and their application in the transesterification of sunflower oil," *Bioresource Technology*, vol. 151, pp. 207–213, 2014.

[31] M. A. C. Teixeira, C. Piccirillo, D. M. Tobaldi et al., "Effect of preparation and processing conditions on UV absorbing properties of hydroxyapatite-Fe_2O_3 sunscreen," *Materials Science & Engineering C*, vol. 71, pp. 141–149, 2017.

[32] S. Mukherjee, S. Dutta, S. Ray, and G. Halder, "A comparative study on defluoridation capabilities of biosorbents: isotherm, kinetics, thermodynamics, cost estimation, and eco-toxicological study," *Environmental Science and Pollution Research International*, vol. 25, no. 18, pp. 17473–17489, 2018.

[33] S. Gogoi, S. K. Nath, S. Bordoloi, and R. K. Dutta, "Fluoride removal from groundwater by limestone treatment in presence of phosphoric acid," *Journal of Environmental Management*, vol. 152, pp. 132–139, 2015.

[34] Y.-S. Ho, "Review of second-order models for adsorption systems," *Journal of Hazardous Materials*, vol. 136, no. 3, pp. 681–689, 2006.

[35] A. A. Izuagie, W. M. Gitari, and J. R. Gumbo, "Synthesis and performance evaluation of Al/Fe oxide coated diatomaceous earth in groundwater defluoridation: towards fluorosis mitigation," *Journal of Environmental Science and Health, Part A: Toxic/Hazardous Substances & Environmental Engineering*, vol. 51, no. 10, pp. 810–824, 2016.